International Journal of Research (IJR)
e-ISSN: 2348-6848, p- ISSN: 2348-795X Volume 2, Issue 12, December 2015
Available at http://internationaljournalofresearch.org

Fuzzy Based Control for an Isolated Inverter through Wound Rotor Machine Fed by a Single-Phase Grid

Anupoju Prathyusha
PG Scholar, Nova College Of Engineering And Technology Jangareddy Gudem , Department Of Electrical And Electronics Engineering , JNTUK Andhra Pradesh, India.
Mr. A. Anjaneyulu
Nova College Of Engineering And Technology Jangareddy Gudem , Department Of Electrical And Electronics Engineering , JNTUK Andhra Pradesh, India.

ABSTRACT

This paper proposes a novel energy conversion system for variable speed drives. It consists of a wound rotor machine and an inverter without any rectifier and input filter. In the proposed system, the stator of the machine is directly connected to a single phase grid and the rotor is connected to three-phase inverter isolated with any external power source. The inverter can not only be connected through slip rings but also integrated on the rotor due to the structure. In this paper, based on the positive and negative sequence model, the rotor, stator powers, and the torque capability in the rotor energy balance and unity grid power factor are analyzed using fuzzy logic controller. From these analyses, the vector control methods of the torque, speed, the dc-link voltage of the isolated inverter, and the grid power factor are proposed. Since the power supplied from the single-phase grid is pulsating and the machine is directly connected to the grid, the controlled torque and power inevitably pulsates at twice the grid frequency. Nevertheless, the machine can start, accelerate, and decelerate in the wide range. The simulation results present the performance and the feasibility of the proposed system using fuzzy logic controller

INTRODUCTION

RECENTLY, ac–ac energy conversion systems with regenerative capability have been widely applied for adjustable speed operation of electric machines in various industries. Many researchers have attempted to achieve high performance, efficiency, and reduced costs of the system [1]–[15]. In these energy conversion systems, a back-to-back system is mostly used because of its simple structure, bidirectional operation capability, and high quality of the grid control.

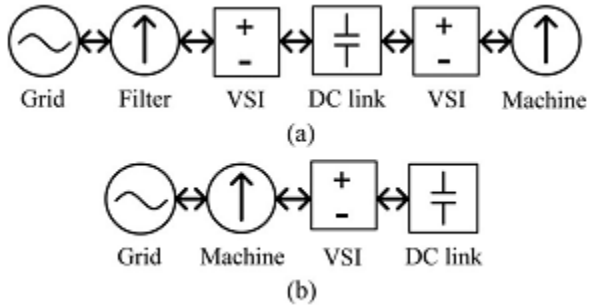

Fig. 1. Energy conversion sequences in (a) the back-to-back system and (b) the proposed system.

The back-to-back system consists of two voltage source inverters (VSIs), a common dc-link capacitor, and an input filter. One of the VSIs is connected to the three-phase machine and controls the current, torque, and/or speed. The other is connected to a grid source, which can be either a single-phase grid or a three-phase grid. It regulates the dc-link voltage and the grid Power Factor (PF). Here, since the switching devices cause current harmonics, the input filter is placed between the grid side VSI and the grid. In the back-to-back system, the machine drive is performed by the machine side VSI only and the other functions, such as regulating the dc-link voltage and the grid current, are executed by the other parts. These parts lengthen the energy conversion sequence of

International Journal of Research (IJR)
e-ISSN: 2348-6848, p- ISSN: 2348-795X Volume 2, Issue 12, December 2015
Available at http://internationaljournalofresearch.org

the system as in Fig. 1(a) and increase the cost, complexity, and losses. In the considerations, doubly fed induction machine (DFIM), in which the stator and rotor windings are connected to the three-phase grid and the back-to-back system, respectively, can be a solution to reduce costs and losses. In DFIM, since only slip power needs to be handled by the back to-back system of the rotor side, the power rating of it can be reduced to 25–30% [16]–[21]. However, the operating range is restricted to the low slip speed range to reduce the slip power, and the energy conversion sequence is longer than in the case of Fig. 1(a), so the total system becomes more complex.

In the recent research, the drive system with the simplified energy conversion sequence as shown in Fig. 1(b) was proposed [22], [23]. In this system, the stator is directly connected to the grid and a single inverter is applied to the rotor, so it can be called a single external feeding of doubly fed wound rotor machine (SEF-DFWM). Compared with the conventional DFIM system, the possible operating area is restricted, but the cost, the complexity, and the energy conversion stages can be reduced. This paper proposes a new drive system applying a single phase grid source. It is inspired by the energy conversion concept of the SEF-DFWM as in Fig. 1(b). This system is called a single external feeding of single-phase doubly fed wound rotor machine (SEF-SDFWM). In SEF-SDFWM, one end of the single-phase grid is directly connected to the stator side a-phase winding, the other end is connected to b- and c-phase windings, and a three-phase inverter is applied to the three-phase rotor windings as shown in Fig. 2(a) and (b). The inverter of the rotor side can be connected to the rotor windings through the slip rings as in Fig. 2(a), or it can be integrated on the rotor shaft as shown in Fig. 2(b) because it has no external power source and connection. Here, the inverter-integration applied in [8] can be used. In this case, the slip rings and brushes are eliminated so the total system structure becomes more compact. The full integration of the inverter requires additional techniques to control the system without any measurement of the stator and external sides. However, the main focus of this paper is not the integration of the rotor-side inverter itself, but the operation principle and the control method of SEF-SDFWM. Therefore, this paper covers the case of Fig. 2(a) only but can be extended to the concept of Fig. 2(b).

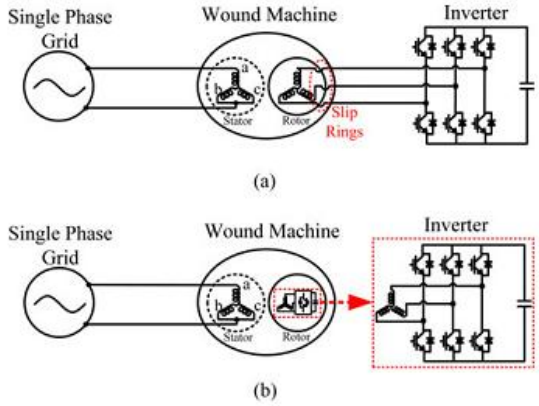

Fig. 2. Two structures of the proposed system: (a) One connected to the inverter by slip rings. (b) One integrating the inverter on the shaft without slip rings.

In this paper, SEF-SDFWM is modeled as the sum of two DFIMs, of which the stator windings are connected to the three phase voltages in the positive and negative sequences, respectively. Based on the rotor currents of these models, the characteristics of the torque, the rotor, and stator powers are analyzed. From these analyses, the control methods of the torque, speed, the dc-link voltage of the rotor-side inverter, and the grid PF are proposed. The experimental results are presented to prove the feasibility of the proposed system

CASE STUDY OF PROPOSED THEORY

MODELING AND FIELD ORIENTATION

A. Modeling of the Single-Phase Grid

While the single-phase grid is directly connected to the stator windings without auxiliary winding as in Fig. 2(a) and (b), the stator flux is not rotating but pulsating [24]–[30]. Since the conventional vector control is based on the rotating flux, it cannot be directly applied to the proposed system. Thus, in this paper, the single-phase grid

International Journal of Research (IJR)
e-ISSN: 2348-6848, p- ISSN: 2348-795X Volume 2, Issue 12, December 2015
Available at http://internationaljournalofresearch.org

voltage connected to the stator windings is modeled as the sum of two three-phase voltages applied to the three-phase windings. The two three-phase voltages are called positive sequence voltages and negative sequence voltages, respectively, which rotate at the same synchronous speed in opposite directions and have the same magnitude. While as the single-phase grid voltage is given by (1), the positive and negative sequence voltages can be represented as in (2) and (3), respectively.

$$V_s = -E\sin(\theta_{\text{grid}}) \quad (1)$$

$$V_{as,p} = -E_p \sin(\theta_{\text{grid}}) = V_{as},$$

$$V_{bs,p} = -E_p \sin\left(\theta_{\text{grid}} - \frac{2}{3}\pi\right), \quad (2)$$

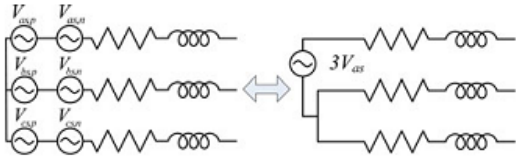

Fig. 3. Relationship between the positive/negative sequence voltages and the single-phase voltage

$$V_{cs,p} = -E_p \sin\left(\theta_{\text{grid}} + \frac{2}{3}\pi\right)$$

$$V_{as,n} = -E_p \sin(\theta_{\text{grid}}) = V_{as}$$

$$V_{bs,n} = -E_p \sin\left(\theta_{\text{grid}} + \frac{2}{3}\pi\right),$$

$$V_{cs,n} = -E_p \sin\left(\theta_{\text{grid}} - \frac{2}{3}\pi\right)$$

Where Ei s the magnitude of the single-phase grid voltage, θ grid denotes the angle of it, the subscript "p" and "n" mean the positive and negative sequence, respectively ,Ep is the magnitude of the modeled three-phase voltages, and the a-phase voltages of them, V as, p and V as, n, are synchronized to the single-phase grid voltage, Vs. Here, Ep can be determined by applying the superposition principle to the modeled three-phase voltages. Since each of them is balanced, the following relations are satisfied:

$$V_{bs,p} + V_{bs,n} = V_{cs,p} + V_{cs,n} = -V_{as}. \quad (4)$$

If the result of (4) is applied, the sum of the positive and negative sequence three-phase voltages can be represented by the single-phase voltage applied between the a-phase and the other phases as shown in Fig. 3. Therefore, each magnitude of the modeled three-phase voltages is determined by a third of the magnitude of the single-phase voltage (Ep =E/3).

B. Positive and Negative Sequence Models of SEF-SDFWM

SEF-SDFWM can be modeled as the sum of two DFIMs, of which the stators are directly connected to the positive and negative sequence three-phase voltages, respectively, and they are called positive and negative sequence models. Here, each of them is exactly the same as the case of the conventional grid connected DFIM. Therefore, the d–q equivalent circuit of the DFIM in the stator flux reference frame can be applied to each of the models as shown in Fig. 4(a) and (b), where the superscripts "p" and "n" denote the positive and negative sequence stator flux reference frames, and ω_p and ω_n are the frequencies of the positive and negative sequence stator fluxes, respectively. Thus, the conventional stator flux oriented vector control for the DFIM in [16]–[21] can be applied to each of them.

C. Field Orientation in the Proposed Vector Control

In the case of the DFIM, the stator flux angle can be obtained from the measured grid voltage without any flux measurements. If the voltage drop by the stator resistance, Rs, is ignored in the stator voltage equation, the following equation can be derived:

$$V_{dqs}^{s} = R_s I_{dqs}^{s} + \frac{d\lambda_{dqs}^{s}}{dt} \approx \frac{d\lambda_{dqs}^{s}}{dt} \quad (5)$$

International Journal of Research (IJR)
e-ISSN: 2348-6848, p- ISSN: 2348-795X Volume 2, Issue 12, December 2015
Available at http://internationaljournalofresearch.org

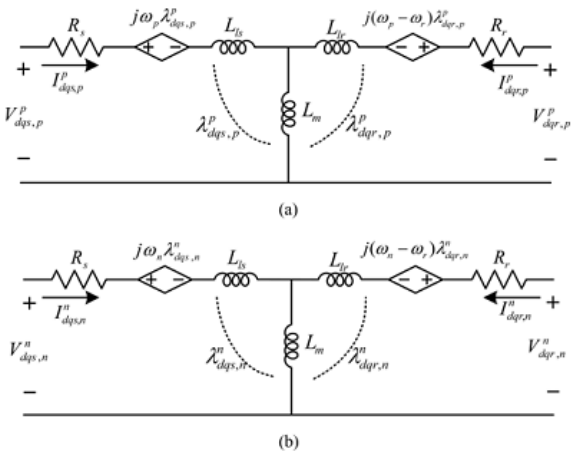

Fig. 4. Equivalent circuits of (a) positive sequence model and (b) negative sequence model.

where the superscript "s" is a stationary reference frame. From (5), it can be deduced that the angle difference between the stator flux and the grid voltage maintains 90 ◦ . Thus, the angle of the stator flux is obtained from the grid voltage, and its frequency becomes the same as the grid frequency,ωg. In the same manner, the angles of the positive and negative sequence stator flux sequence stator fluxes, $\theta_{sf,p}$ and$\theta_{sf,n,}$ are approximated as θ_{grid} and$-\theta_{grid,}$ and the frequencies of them, ω_p andω_n,are approximated as ω_g and $-\omega_g$, respectively.

$$\theta_{sf,p} \approx \theta_{grid}, \theta_{sf,n} \approx -\theta_{grid}, \omega_p \approx \omega_g, \omega_n \approx -\omega_g. \quad (6)$$

Therefore, θ_{grid} and$-\theta_{grid}$ can be used as the field orientation angles of the positive and negative sequence stator flux reference frames, respectively.

CHARACTERISTICS OF SEF-SDFWM

As mentioned previously, SEF-SDFWM is modeled as the sum of the positive and negative sequence models. Hence, from the models, the components of the proposed system can be determined. This section presents the characteristics of SEFSDFWM such as the torque, stator and rotor powers based on the models. The torque capability considering the grid PF regulation and the stabilization of the dc-link voltage is also analyzed.

A. Torque Characteristics of SEF-SDFWM

Torque of the electric machine can be determined by the currents and fluxes. In DFIM, the torque can be represented by rotor currents and stator fluxes as follows

$$T_e = \frac{3}{2}\frac{P}{2}\frac{L_m}{L_s}\,\mathrm{Im}\{(\lambda^{\omega}_{dqs})(I^{\omega}_{dqr})^*\} \quad (7)$$

where the superscript "ω" is an arbitrary reference frame, Im{•} means an imaginary part of{•}, and the superscript " ∗ " denotes the complex conjugate. In SEF-SDFWM, since the stator fluxes and the rotor currents can be determined by sum of the positive and negative sequence models, the torque can be divided into four components as follows

$$T_{e,pp} = \frac{3}{2}\frac{P}{2}\frac{L_m}{L_s}\,\mathrm{Im}\{\lambda^{p}_{dqs,p} I^{p*}_{dqr,p}\} = \frac{3}{2}\frac{P}{2}\frac{L_m}{L_s}\lambda^{p}_{ds,p}(-I^{p}_{qr,p}) \quad (8)$$

$$T_{e,nn} = \frac{3}{2}\frac{P}{2}\frac{L_m}{L_s}\,\mathrm{Im}\{\lambda^{n}_{dqs,n} I^{n*}_{dqr,n}\} = \frac{3}{2}\frac{P}{2}\frac{L_m}{L_s}\lambda^{n}_{ds,n}(-I^{n}_{qr,n}) \quad (9)$$

$$\begin{aligned} T_{e,pn} &= \frac{3}{2}\frac{P}{2}\frac{L_m}{L_s}\,\mathrm{Im}\{\lambda^{p}_{dqs,p}(e^{-j2\theta_{\mathrm{grid}}} I^{n}_{dqr,n})^*\} \\ &= \frac{3}{2}\frac{P}{2}\frac{L_m}{L_s}\lambda^{p}_{ds,p}(I^{n}_{dr,n}\sin(2\theta_{\mathrm{grid}}) - I^{n}_{qr,n}\cos(2\theta_{\mathrm{grid}})) \end{aligned} \quad (10)$$

$$\begin{aligned} T_{e,np} &= \frac{3}{2}\frac{P}{2}\frac{L_m}{L_s}\,\mathrm{Im}\{\lambda^{n}_{dqs,n}(e^{j2\theta_{\mathrm{grid}}} I^{p}_{dqr,p})^*\} \\ &= \frac{3}{2}\frac{P}{2}\frac{L_m}{L_s}\lambda^{n}_{ds,n}(-I^{p}_{dr,p}\sin(2\theta_{\mathrm{grid}}) - I^{p}_{qr,p}\cos(2\theta_{\mathrm{grid}})) \end{aligned} \quad (11)$$

Where Te, pp is the torque by the positive sequence fluxes and currents, Te,nn by the negative sequence currents and fluxes, Te,pn by the positive sequence fluxes and the negative sequence currents, Te,np by the negative sequence fluxes and the positive sequence currents, and the coordinate transformations into the negative and positive sequence stator flux reference frames are applied to the rotor currents of Te,pn and Te,np to use I n∗ dqr,n and Ip∗ dqr,p instead of I p∗dqr,n and I n∗ dqr,p , respectively. In each of the positive and negative sequence stator flux reference frames, the q-axis stator flux becomes zero and the d-axis stator flux is consistent, where the grid is constant. The value corresponds to the magnitude of the stator flux and can be determined by the ratio of the grid voltage to the grid frequency from (5). Therefore, if (5) is applied to the models, each of

International Journal of Research (IJR)
e-ISSN: 2348-6848, p- ISSN: 2348-795X Volume 2, Issue 12, December 2015
Available at http://internationaljournalofresearch.org

the d-axis stator fluxes in the models can be decided by the ratio of Ep to the grid frequency as follows:

$$\lambda^{p}_{ds,p} \approx \lambda^{n}_{ds,n} \approx \frac{E_p}{\omega_g} = \frac{E}{3\omega_g}. \quad (12)$$

The torque of SEF-SDFWM becomes a function of the rotor currents. If the rotor currents are controlled in each of synchronous frames, the torques of (8)–(11) can be classified into two categories; ripple torque,Tripple, and effective torque, Teff

$$T_{\text{ripple}} = T_{e,pn} + T_{e,np} \approx \frac{3}{2}\frac{P}{2}\frac{L_m}{L_s}\frac{E}{3\omega_g}\{(I^{n}_{dr,n} - I^{p}_{dr,p})\sin(2\theta_{\text{grid}}) - (I^{n}_{qr,n} + I^{p}_{qr,p})\cos(2\theta_{\text{grid}})\} \quad (13)$$

$$T_{\text{eff}} = T_{e,pp} + T_{e,nn} \approx -\frac{3}{2}\frac{P}{2}\frac{L_m}{L_s}\frac{E}{3\omega_g}(I^{p}_{qr,p} + I^{n}_{qr,n}) = K_T(I^{p}_{qr,p} + I^{n}_{qr,n}) \quad (14)$$

Where KT is the torque constant. The sum of Te,pn andTe,np produces the ripple torque, of which the frequency is twice the grid frequency, 2ωg. This ripple torque by the pulsating

TABLE I
SYSTEMPARAMETERS
ANDGRIDCONDITIONS

Rated power	800W	Rated speed	1720r/min
Stator resistance (R_s)	0.6Ω	Rated torque	4.2Nm
Rotor resistance (R_r)	0.7Ω	Rated current	6Arms
Stator inductance (L_s)	54mH	Number of poles	4
Rotor inductance (L_r)	56mH	Grid voltage	110Vrms
Mutual inductance (L_m)	49mH	Grid frequency	60Hz
Dc link capacitance	680μF	Inertia of Exp. set-up	0.112 kg·m²

stator flux mentioned previously causes the speed ripple of the system. However, it has no effect on the average level of the speed. Also, as the inertia of the system increases, the ripple effect decreases. On the other hand, the sum ofTe,ppandTe,nn generates the effective torque, which is proportional to the torque constant and the sum of the positive and negativeq-axis rotor currents. The effective torque determines the average speed, so in this paper, only the effective torque is considered for the torque control. Therefore, since the ignored ripple torque of (13) results in the ripple speed, the application of the proposed system should be cautiously decided and additional inertia may be required to reduce the ripple effect. The machine parameters and the single-phase grid conditions used in the simulation are listed in Table I. The shapes of those curves are not perfectly linear because the positive and negative sequenced-axis stator fluxes have small effect from the rotor currents. This variation of the stator flux can result in torque errors, but it is less than 10% of the value of (12) and these errors can be compensated by the stator flux estimation or lookup table.

B. PF of the Grid

In the grid-connected system, the grid PF should be regulated. In the DFIM systems, the stator active and reactive powers can be controlled by one-rotor current vector, and this makes the PF regulated [16]–[21]. The proposed system has two-rotor current vectors, which are the positive and negative sequence rotor current vectors. Thus, the increased current vectors are considered for the PF regulation. Since the grid-side current of the proposed system flows through the a-phase winding as shown in Fig. 2, it is determined by thed-axis stator current in the stationary reference frame. Thus, in the proposed system, the grid side current is obtained as follows.

$$I_s = \sin(\theta_{\text{grid}})\frac{L_m}{L_s}(I^{p}_{qr,p} - I^{n}_{qr,n}) + \cos(\theta_{\text{grid}})\left\{\frac{\lambda^{p}_{ds,p} + \lambda^{n}_{ds,n} - L_m(I^{p}_{dr,p} + I^{n}_{dr,n})}{L_s}\right\}. \quad (17)$$

The first term of the right side in (17) is in phase with the grid voltage of (1) and becomes an active current supplying the active power. On the other hand, the second term is in quadrature with the grid voltage and becomes a reactive current supplying the reactive power. From these currents and the grid voltage of (1), the values of the stator active power,Ps, and the stator reactive power,Qs, can be obtained as follows:

International Journal of Research (IJR)
e-ISSN: 2348-6848, p- ISSN: 2348-795X Volume 2, Issue 12, December 2015
Available at http://internationaljournalofresearch.org

$$P_s = -\frac{1}{2}E\frac{L_m}{L_s}\left(I^p_{qr,p} - I^n_{qr,n}\right) \quad (18)$$

$$Q_s = -\frac{1}{2}E\left\{\frac{\lambda^p_{ds,p} + \lambda^n_{ds,n} - L_m\left(I^p_{dr,p} + I^n_{dr,n}\right)}{L_s}\right\}. \quad (19)$$

Since the active power of (18) is a sole power source in the total system, it is varied according to rotating speed and torque of the machine. Hence, in order to satisfy the PF regulation of the grid code regardless of the operating condition, the reactive power control is required and can be achieved by sum of the positive and negative sequenced-axis rotor currents based on (19). For example, unity PF or zero reactive power control is accomplished, where sum of thed-axis rotor currents satisfies the following condition

$$I^p_{dr,p} + I^n_{dr,n} = \frac{\lambda^p_{ds,p} + \lambda^n_{ds,n}}{L_m} \approx \frac{2E}{3\omega_g L_m}. \quad (20)$$

Because the sum of thed-axis rotor currents is only decided for a specific stator reactive power, there are many combinations of them. In this paper, the combination for reducing the torque ripple is recommended as follows

$$I^p_{dr,p} = I^n_{dr,n}. \quad (21)$$

In the proposed system, thed–qaxis rotor currents in the positive and negative sequences cause the ripple torque as in (13). To generate the effective torque, the torque ripple by theq-axis rotor currents is inevitable, but that by thed-axis rotor currents can be removed by making the samed-axis rotor currents as in (21).

C. Energy Balance of the Rotor-Side Inverter

As mentioned previously, the rotor-side inverter connected tothe rotor has no external power source. Therefore, unlike the conventional vector control of DFIM, additional considerations about the dc-link voltage regulation are needed in the inverter. In this system, the dc-link voltage depends on the rotor power only from the rotor windings through the rotor-side inverter. Here, the rotor power includes powers consumed in the rotorside inverter, such as losses of the switching device and the control board power consumptions, but these powers are assumed to be relatively small and ignored. Even if these powers are large, the dc-link voltage controller proposed in the paper can compensate it. Therefore, the rotor power can be determined by the positive and negative sequence rotor voltages and currents, V p dqr,p ,V n dqr,n ,I p dqr,p , andI n dqr,n . Like the case of the torque, the rotor power has the following four components

$$\begin{aligned} P_{r,pp} &= \frac{3}{2}\mathrm{Re}\{V^p_{dqr,p}(I^p_{dqr,p})^*\} \\ &= \frac{3}{2}\left(R_r I^{p2}_{dr,p} + R_r I^{p2}_{qr,p} + \frac{L_m}{L_s}s_p\omega_p\lambda^p_{ds,p}I^p_{qr,p}\right) \end{aligned} \quad (22)$$

$$\begin{aligned} P_{r,nn} &= \frac{3}{2}\mathrm{Re}\{V^n_{dqr,n}(I^n_{dqr,n})^*\} \\ &= \frac{3}{2}\left(R_r I^{n2}_{dr,n} + R_r I^{n2}_{qr,n} + \frac{L_m}{L_s}s_n\omega_n\lambda^n_{ds,n}I^n_{qr,n}\right) \end{aligned} \quad (23)$$

$$\begin{aligned} P_{r,pn} &= \frac{3}{2}\mathrm{Re}\{V^p_{dqr,p}(e^{-j2\theta_{\mathrm{grid}}}I^n_{dqr,n})^*\} \\ &= \frac{3}{2}\{\sin(2\theta_{\mathrm{grid}})(V^p_{dr,p}I^n_{qr,n} - V^p_{qr,p}I^n_{dr,n}) \\ &\quad + \cos(2\theta_{\mathrm{grid}})(V^p_{dr,p}I^n_{dr,n} + V^p_{qr,p}I^n_{qr,n})\} \end{aligned} \quad (24)$$

$$\begin{aligned} P_{r,np} &= \frac{3}{2}\mathrm{Re}\{V^n_{dqr,n}(e^{j2\theta_{\mathrm{grid}}}I^p_{dqr,p})^*\} \\ &= \frac{3}{2}\{\sin(2\theta_{\mathrm{grid}})(-V^n_{dr,n}I^p_{qr,p} + V^n_{qr,n}I^p_{dr,p}) \\ &\quad + \cos(2\theta_{\mathrm{grid}})(V^n_{dr,n}I^p_{dr,p} + V^n_{qr,n}I^p_{qr,p})\} \end{aligned} \quad (25)$$

where Re{•}means a real part of{•}, Pr,pp is the rotor power by the positive sequence rotor voltages and currents,Pr,nn is the rotor power by the negative sequence rotor voltages and currents,Pr,pn is the rotor power by the positive sequence rotor voltages and the negative sequence rotor currents, Pr,np is the rotor power by the negative sequence rotor voltages and the positive sequence rotor currents, andsp andsn are the positive and negative sequence slips, which are defined by (ωp − ωr)/ωp and (ωn −ωr)/ωn, respectively. Also, the coordinate transformations into the negative and positive sequence stator flux reference frames are applied to the rotor currents ofPr,pn andPr,np in order to useI n∗ dqr,n andI p∗ dqr,p instead ofI dqr,n and I n∗ dqr,p , respectively. Those rotor powers can be classified into two

International Journal of Research (IJR)
e-ISSN: 2348-6848, p- ISSN: 2348-795X Volume 2, Issue 12, December 2015
Available at http://internationaljournalofresearch.org

categories; ripple rotor power,Pr,ripple, and effective rotor power,Pr,e

$$P_{r,\text{ripple}} = P_{r,pn} + P_{r,np} \quad (26)$$

$$P_{r,\text{eff}} = P_{r,pp} + P_{r,nn}. \quad (27)$$

The sum ofPr,pn andPr,np produces the ripple rotor power, of which the frequency is twice the grid frequency. This ripple rotor power causes the ripple in the dc-link voltage but has no effect on average value of the dc-link voltage. Besides, as th capacity of the dc link increases, the voltage ripple decreases. On the other hand, the sum ofPr,pp andPr,nn generates the effective rotor power, which can regulate the dc-link voltage, so in this paper, only the effective rotor power is considered for the dc-link voltage control. Thus, the large capacitance may be required to smooth the ripple of the dc-link voltage, but when the large capacitor size of the normal single-phase source system to endure the power ripple is considered, the capacitor size in the proposed system is not such a large penalty. WheneverPr,eff > 0, the energy of the dc link is supplied to the rotor winding so the voltage of the dc link decreases. WherePr,eff <0, the voltage increases. Where Pr,eff =0, the energy of the inverter is balanced and the dc-link voltage is maintained. This means that the dc-link voltage can be controlled by the effective rotor power. The effective rotor power becomes the function of the rotor currents at a certain slip speed as shown in (22) and (23). However, since thed-axis rotor currents cause copper losses only, they cannot be the active factors for bidirectionally controlling the effective rotor power. Also, they are determined for the stator reactive power control, so the q-axis rotor currents become the active factors for controlling the effective rotor power. Assumed that thed-axis rotor currents are regulated to satisfy the conditions of (20) and (21), the equation thatPr,eff =0 can be

written in the steady state as follows:

$$\left(I^p_{qr,p} + \frac{L_m\omega_g\lambda^p_{ds,p}s_p}{2L_sR_r}\right)^2 + \left(I^n_{qr,n} - \frac{L_m\omega_g\lambda^n_{ds,n}s_n}{2L_sR_r}\right)^2$$
$$= \left(\frac{L_m\omega_g}{2L_sR_r}\right)^2\{(\lambda^p_{ds,p}s_p)^2 + (\lambda^n_{ds,n}s_n)^2\} - 2R_r\left(\frac{E}{3\omega_gL_m}\right)^2. \quad (28)$$

In a specific slip condition, (28) becomes an equation for a circle on the positive and negative sequenceq-axis rotor current plane, assuming that the stator fluxes are constant. Fig. 6(a) and (b) show theq-axis rotor current trajectories of zero effective rotor power at the several slips, where the conditions of Table I are applied andωNdenotes the normalized speed

$$\omega_N = \frac{\omega_r}{\omega_p} \approx \frac{\omega_r}{\omega_g}. \quad (29)$$

According to the speeds, the center points and radiuses of the circles are changed as in (28)

D. Possible Operating Area and Torque Capability

The operating points on theq-axis rotor current plane satisfy both conditions of the desired torque and the zero effective rotor power for constant dc-link voltage, where the PF is regulated by thed-axis rotor currents. In addition, these operating points are within the rotor current limit considering the thermal issue. In controlling each of the rotor currents in the positive and negative sequences, the RMS value of the rotor current can be calculated as follows:

$$\text{RMS}(I_r) = \frac{\sqrt{I_p^2 + I_n^2}}{\sqrt{2}} \quad (30)$$

whereIp andIn are the vectors of the rotor currents in the positive and negative sequences, respectively, andIr denotes the total rotor current vector. Thus, the current limit of the qaxis rotor currents can be set as follows:

$$I^{p^2}_{qr,p} + I^{n^2}_{qr,n} \le (\sqrt{2}I_{\text{rated\_RMS}})^2 - (I^{p^2}_{dr,p} + I^{n^2}_{dr,n}) \quad (31)$$

Where Irated RMS denotes the RMS value of the rated rotor current. Along with the current limit, curves of constant torque and zero effective rotor power are drawn in Fig. 7, where the d-axis rotor currents are determined in the conditions of

International Journal of Research (IJR)
e-ISSN: 2348-6848, p- ISSN: 2348-795X Volume 2, Issue 12, December 2015
Available at http://internationaljournalofresearch.org

(20) and (21). Also this point should be in the current limit circle. If the intersection is formed in the outer region of the current limit circle, the operating point should be moved into the boundary of the circle, satisfying the zero effective rotor power condition, and it restricts the torque generation. It means that the dc-link voltage control has priority over the torque control because the dc-link voltage control is directly related to stability of the total system. Therefore, where the dc-link voltage is regulated to constant level, the maximum torque at a specific speed is determined by the intersection of the current limit circle and the zero effective rotor power curve of the speed.

For the comparison with the conventional system, the capability of a vector-controlled threephase squirrel cage induction machine is also presented, where the dc-link voltage is fixed to the magnitude of the single-phase grid. In the low-speed range where$|\omega N|<1.5$, the proposed system has the lower torque than that of the three-phase squirrel cage induction machine. On the other hand, in the high-speed range where$|\omega N|>2$, SEF-SDFWM can generate the higher torque than the three-phase squirrel cage induction machine because the proposed system can boost the dc-link voltage by the rotor-side inverter without any additional device.

FUZZY LOGIC CONTROLLER

INTRODUCTION TO FUZZY

Fuzzy logic theory is considered as a mathematical approach combining multi-valued logic, probability theory, and artificial intelligence to replicate the human approach in reaching the solution of a specific problem by using approximate reasoning to relate different data sets and to make decisions. The performance of Fuzzy Logic Controllers is well documented in the field of control theory since it provides robustness to dynamic system parameter variations as well as improved transient and steady state performances. In this study, a fuzzy logic based feedback controller is employed for controlling the voltage injection of the proposed Dynamic Voltage Restorer (DVR). Fuzzy logic controller is preferred over the conventional PI and PID controller because of its robustness to system parameter variations during operation and its simplicity of implementation. Since the proposed DVR uses energy storage system consisting of capacitors charged directly from the supply lines through rectifier and the output of the inverter depends upon the energy stored in the dc link capacitors. But as the amount of energy stored varies with the voltage sag/swell events, the conventional PI and PID controllers are susceptible to these parameter variations of the energy storage system; hence the control of voltage injection becomes difficult. The proposed FLC scheme exploits the simplicity of the Mamdani type fuzzy systems that are used in the design of the controller and adaptation mechanism.

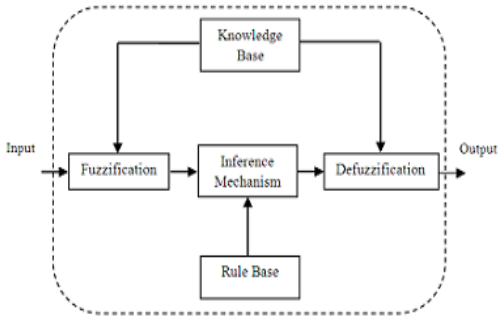

Figure. Schematic representation of Fuzzy Logic Controller

The fuzzy logic based control scheme (Fig) can be divided into four main functional blocks namely Knowledge base, Fuzzification, Inference mechanism and Defuzzification. The knowledge base is composed of data base and rule base. Data base consists of input and output membership functions and provides information for appropriate fuzzification and defuzzification operations.

The rule-base consists of a set of linguistic rules relating the fuzzified input variables to the desired control actions. Fuzzification converts a crisp input signals, error (e), and change in error (ce) into fuzzified signals that can be identified by level of memberships in the fuzzy sets. The inference

International Journal of Research (IJR)
e-ISSN: 2348-6848, p- ISSN: 2348-795X Volume 2, Issue 12, December 2015
Available at http://internationaljournalofresearch.org

mechanism uses the collection of linguistic rules to convert the input conditions to fuzzified output. Finally, the defuzzification converts the fuzzified outputs to crisp control signals using the output membership function, which in the system acts as the changes in the control input (u).The typical input membership functions for error and change in error are shown in Fig respectively, whereas the output membership function for change in control input is shown in Fig 8c. The output generated by fuzzy logic controller must be crisp which is used to control the PWM generation unit and thus accomplished by the defuzzification block. Many defuzzification strategies are available, such as, the weighted average criterion, the mean-max membership, and center-of-area (centroid) method. The defuzzification technique used here is based upon centroid method.

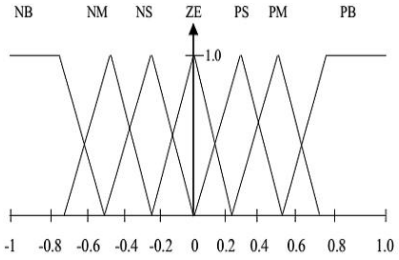

Figure. Membership Function for Input Variable Error, ‘e’

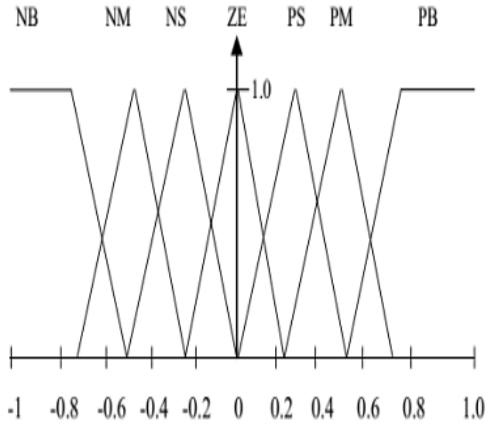

Figure. Membership Function for Input Variable Change in Error, ‘ce’

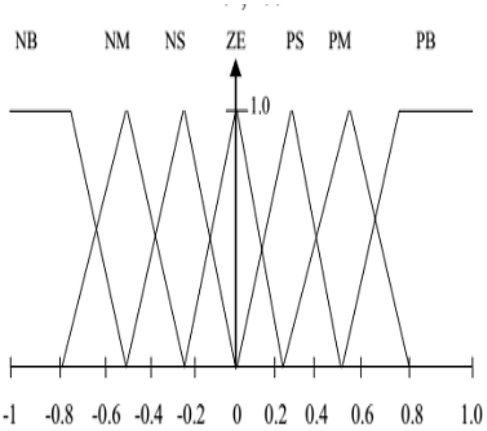

Figure. Membership Function for Output Variable Change in Control Signal, ‘u’.

The set of fuzzy control linguistic rules is given in Table 1. The inference mechanism of fuzzy logic controller utilizes these rules to generate the required output. DVR is generally connected in feeders having sensitive loads whose terminal voltage has to be regulated. The SIMULINK model of proposed fuzzy logic controller is shown in the Fig .

Table 1. Rule Base for Fuzzy Logic Controller

‘e’ / ‘ce’	NB	NM	NS	ZE	PS	PM	PB
NB	NB	NB	NB	NB	NM	NS	ZE
NM	NB	NB	NB	NM	NS	ZE	PS
NS	NB	NB	NM	NS	ZE	PS	PM
ZE	NB	NM	NS	ZE	PS	PM	PB
PS	NM	NS	ZE	PS	PM	PB	PB
PM	NS	ZE	PS	PM	PB	PB	PB
PB	ZE	PS	PM	PB	PB	PB	PB

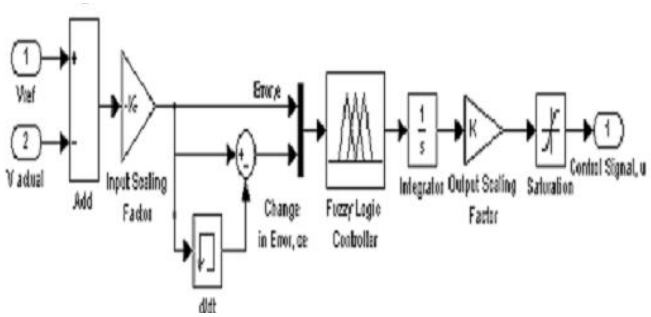

Figure. SIMULINK model of proposed FLC

International Journal of Research (IJR)
e-ISSN: 2348-6848, p- ISSN: 2348-795X Volume 2, Issue 12, December 2015
Available at http://internationaljournalofresearch.org

RESULTS

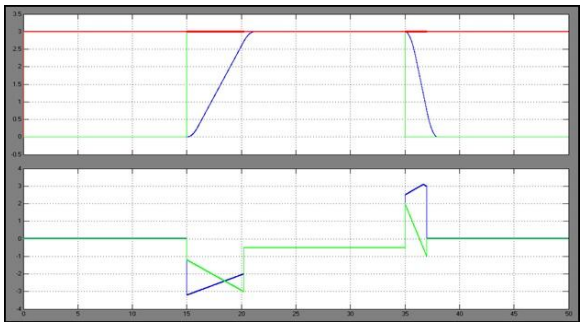

Fig. 15. Performances of the speed and the dc-link voltage controls with step variations of the rotating speed reference from zero via 1800 r/min to zero. (a) Rotating speed, its reference, and dc-link voltage. (b) References of the torque and voltage component currents, and their Lissajous figure

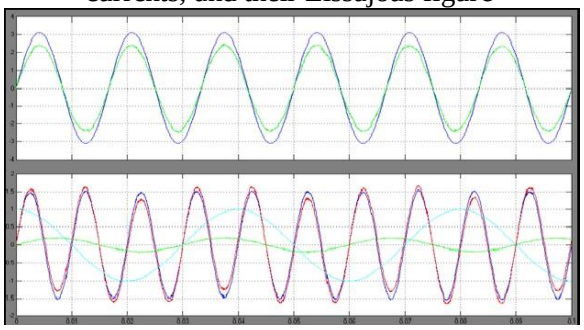

Fig. 16. Voltages and currents of the stator and rotor sides at 900 r/min with rated load torque. (a) Measured voltage and current of the stator. (b) References of the positive and negative sequence voltages, their sum in the rotor reference frame, and measured *d*-axis rotor current.

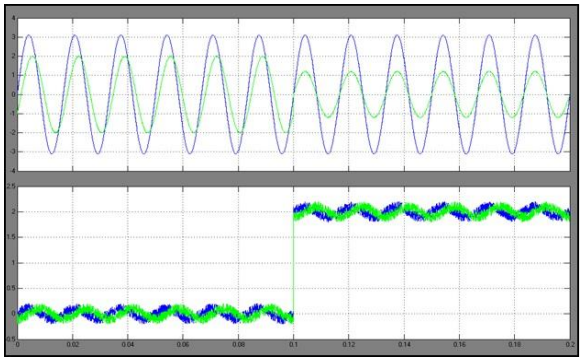

Fig. 17. Performances of the speed, the dc-link voltage, the PF controls at
900 r/min with step-rated load torque. (a) Rotating speed, dc-link voltage, and
references of the torque and voltage component currents. (b) Stator voltage and
current.

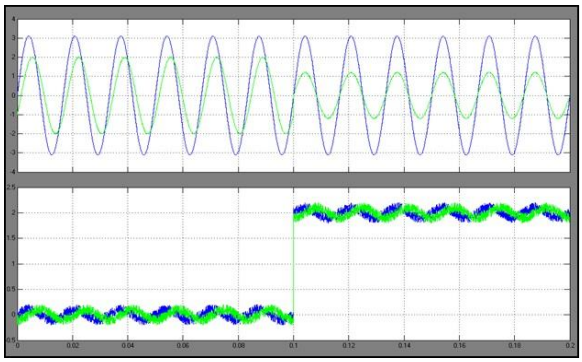

Fig. 18. PF control performance at 900 r/min with half-rated load torque. (a) Stator voltage and current. (b) Positive and negative sequence *d*-axis rotor currents.

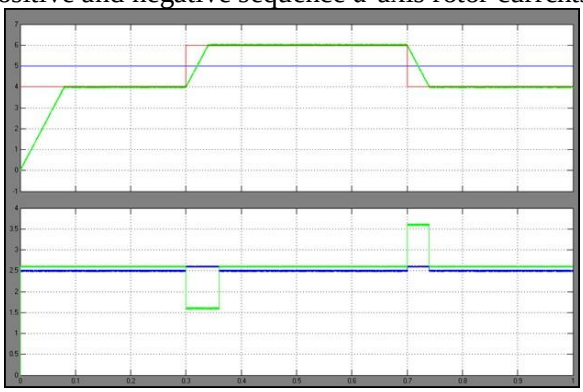

Fig. 19. Dc-link voltage control performance, where the reference of the dclink voltage is changed from 200 V via 300 to 200 V. (a) Dc-link voltage, its reference, and rotating speed. (b) References of the torque and voltage component currents.

CONCLUSION

This paper has presented a configuration of SEF-SDFWM and the control method. The stator is directly connected to the singlephase grid and the rotor is connected to the three-phase inverter, which is not fed by any other external power source. Since the proposed control methods include the ripple components from the pulsating stator flux and the grid power is directly converted, the considerations for the precise control applications or the systems which are vulnerable to the disturbance are required. However, the proposed system uses only one rotor-side inverter and does not require any rectifier and input filter. Additionally,since the inverter is isolated from the grid, the inverter can be integrated into the rotor shaft. Thus, the brushes and slip rings of the conventional DFIMs can be eliminated. The

system structure is compact and can reduce the cost and size of the total system. The proposed system is modeled as the sum of two DFIMs, of which the stator windings are connected to the three-phase voltages in the positive and negative sequences, respectively. Based on these models, the torque, rotor power, and stator power are analyzed and the vector control methods of the speed, dc-link voltage, and the grid PF are proposed. Further, the estimation of the stator flux can be added to enhance the control performance and endure the grid disturbance.

REFERENCES

[1] B. Metidji, N. Taib, L. Baghli, T. Rekioua, and S. Bacha, "Low-cost direct torque control algorithm for induction motor without AC phase current sensors,"IEEE Trans. Power Electron., vol. 27, no. 9, pp. 4132–4139, Sep. 2012.

[2] A. Yoo, S. Sul, H. Kim, and K. Kim, "Flux-weakening strategy of an induction machine driven by an electrolytic-capacitor-less inverter,"IEEE Trans. Ind. Appl, vol. 47, no. 3, pp. 147–154, May/Jan. 2011.

[3] K. Inazuma, H. Utsugi, K. Ohishi, and H. Haga, "High-power-factor single-phase diode rectifier driven by repetitively controlled IPM motor," IEEE Trans. Ind. Electron., vol. 60, no. 10, pp. 4427–4437, Oct. 2013.

[4] H. Lee, S. Jung, and S. Sul, "A current controller design for current source inverter-fed AC machine drive system," IEEE Trans. Power Electron., vol. 28, no. 3, pp. 1366–1381, Mar 2013.

[5] S. Khwan-on, L. Lillo, L. Empringham, and P. Wheeler, "Fault-tolerant matrix converter motor drives with fault detection of open switch faults," IEEE Trans. Ind. Electron., vol. 59, no. 1, pp. 257–268, Jan. 2012.

[6] J. Ewanchuk, J. Salmon, and C. Chapelsky, "A method for supply voltage boosting in an open-ended induction machine using a dual inverter system with a floating capacitor bridge,"IEEE Trans. Power Electron., vol. 28, no. 3, pp. 1348–1357, Mar 2013.

[7] S. Kouro, M. Malinowski, K. Gopakumar, J. Pou, L. G. Franquelo, B. Wu, J. Rodriguez, M. A. Perez, and J. I. Leon, "Recent advances and industrial applications of multilevel converters,"IEEE Trans. Power Electron., vol. 57, no. 8, pp. 2553–2580, Aug 2010.

[8] E. Jung, S. Kim, J. Ha, and S. Sul, "Control of a synchronous motor with an inverter integrated rotor,"IEEE Trans. Ind. Appl., vol. 48, no. 6, pp. 1993–2001, Jan./Feb. 2012.

[9] P. Guglielmi, B. Boazzo, E. Armando, and G. Pellegrino, "Permanentmagnet minimization in PM-assisted synchronous reluctance motors for wide speed range,"IEEE Trans. Ind. Appl., vol. 49, no. 1, pp. 31–41, Jan./Feb. 2013.

[10] Y. Zhang and J. Zhu, "Direct torque control of permanent magnet synchronous motor with reduced torque ripple and commutation Frequency," IEEE Trans. Power Electron., vol. 26, no. 1, pp. 235–248, Jan. 2011.

[11] V. P. Vujiˇ ci´ c, "Minimization of torque ripple and copper losses in switched reluctance drive,"IEEE Trans. Power Electron., vol. 27, no. 1, pp. 388– 399, Jan. 2012.

[12] A. B. Jidin, N. R. B. N. Idris, A. H. B. M. Yatim, M. E. Elbuluk, and T. Sutikno, "A wide-speed high torque capability utilizing overmodulation strategy in DTC of induction machines with constant switching frequency controller,"IEEE Trans. Power Electron., vol. 27, no. 5, pp. 2566–2575, May 2012.

[13] S. Yang and R. D. Lorenz, "Surface permanent magnet synchronous machine position estimation at low speed using eddy-current-reflected asymmetric resistance,"IEEE Trans.

Power Electron., vol. 27, no. 5, pp. 2595– 2604, May 2012.

[14] S. Kim, Y. Yoon, S. Sul, and K. Ide, "Maximum torque per ampere (MTPA) control of an IPM machine based on signal injection considering inductance saturation," IEEE Trans. Power Electron., vol. 28, no. 1, pp. 488– 497, Jan. 2013.

[15] S. Jung, J. Hong, and K. Nam, "Current minimizing torque control of the IPMSM using Ferrari's method,"IEEE Trans. Power Electron., vol. 28, no. 12, pp. 5603–5617, Dec. 2013.

[16] L. Gao, B. Guan, Y. Zhou, and L. Xu, "Model reference adaptive system observer based sensorless control of doubly-fed induction machine," in Proc. Int. Conf. Electr. Mach. Syst., Oct. 2010, pp. 931–936.

[17] S. M¨ uller, M. Deicke, and R. W. De Doncker, "Doubly fed induction generator systems for wind turbines,"IEEE Trans. Ind. Appl. Mag.,vol.8, no. 3, pp. 26–33, May/Jun. 2002.

[18] A. Doria-Cerezo, "Comments on "Control and performance of a doublyfed induction machine intended for a flywheel energy storage system," IEEE Trans. Power Electron., vol. 28, no. 1, pp. 605–606, Jan. 2013.

[19] R. Cardenas, R. Pena, J. Clare, and G. Asher, "MRAS observers for sensorless control of doubly-fed induction generators,"IEEE Trans. Power Electron., vol. 23, no. 3, pp. 1075–1084, May 2008.

[20] H. Chaal and M. Jovanovic, "Toward a generic torque and reactive power controller for doubly fed machines,"IEEE Trans. Power Electron., vol. 27,no. 1, pp. 113–121, Jan. 2012.